TECHNISCHE MECHANIK, 31, 1, (2011), 1 – 14
submitted: February 2, 2010

Viscoelastic-plastic Modelling and Experimental Investigation of Three Different Batches of 51CrV4 Steel

A. Abid (Al-Baldawi), L. Schreiber

Steel producers, when producing steel with special mechanical properties, always refer to DIN or ISO standards. But these standards only specify the alloying constituents in intervals and only compel producers to guarantee minimal values of mechanical properties e.g. the yield stress. This leads to different mechanical behavior in different batches of steel which is nominally the same. This paper deals with the investigation of the mechanical behavior of three different batches of 51CrV4 and the consequences for their viscoelastic-plastic modelling.

1 Introduction

Phenomenological modelling of material behavior is a aspect of continuum mechanics (Svendsen (1996)). This part is becoming more and more important because of the increasing use of numerical simulation. Inaddition to the balance equation, every simulation needs a model to give the correct dependence between stress and strain because every material behaves differently under mechanical loading.

All advanced models, e.g. Haupt (2000), that relate the stress tensor $\mathbf{T}$ to the strain tensor $\mathbf{E} = \mathbf{E}\big(\mathbf{u}(t)\big)$, $\mathbf{u}$: displacement field , and some internal variables $\mathbf{Q}$ of different order, need several material parameters, for the sake of this paper collected in a parameter vector $\mathbf{p} = (p_i)$, finally we can write:

$$\mathbf{T}(t) = \int \dot{\mathbf{T}}\big(\mathbf{E}(t), \dot{\mathbf{E}}(t), \overset{(n)}{\mathbf{Q}}; \mathbf{p}\big)\, \mathrm{d}t. \tag{1}$$

After integrating (1) in time, a second integration of stress across a certain cross section A of the body leads to the simulated force F_{sim} normal to the cross section:

$$F_{\mathrm{sim}} = \int_A \sigma_{xx}\, \mathrm{d}A. \tag{2}$$

In order to identify material parameters several types of experiments are needed (Haupt (2000), Chakrabarty (2006) and Kreissig (1996)). To get the best set of parameters p_i we need an improvement strategy that fits $F_{\mathrm{sim}}\,(u,t)$ to the measured forces $F_{\mathrm{meas}}\,(u,t)$. To this end we used a software tool based on the Evolution Strategy that was developed by Schreiber (1993). Figure-1 shows (schematically for a three dimensional parameter vector) how to obtain new parameter sets using evolution mechanism with a random generator in order to gain new parameters in the sets. The way to the best parameter set is governed by the least sqares method applied to the difference between experimentally measured forces and those simulated according to the actual parameter set.

We used a tension compression test in several versions, A-E, to get all material parameters needed, see Figure-2.

Test A is very useful to allow a first look at the material behavior and also to obtain an initial parameter set for the ensuing identification process. In order to minimize viscous phenomena (in other words, to stay near the 'equilibrium state'), it is neccessary to drive a slow version of test A, which here is called test B. This test is important for the parameters that describe the (non-viscous) hardening behavior.

To gain an overview of the relaxation of the material we used a classic relaxation test, here called test C. This test is needed to fit the parameters included in the model to describe the time dependent part of stress.

In conclusion, we wanted to gain more information on the equilibrium hysteresis, therefore we carried out two step tests, one in the tension region and the other in the compression region, called test D and E. These two tests helped to do the last fine tuning on the whole parameter set.

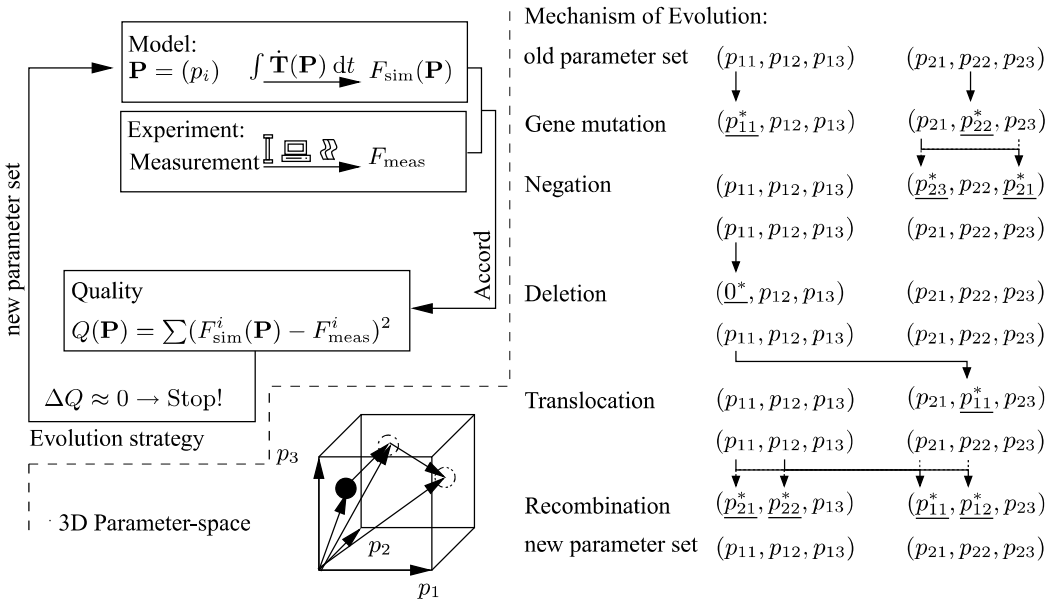

Figure 1: Sketch of the evolution strategy – using evolution mechanism to obtain new parameter sets (right side) and the least squares method as an accord mechanism (left side), see Schreiber (1993)

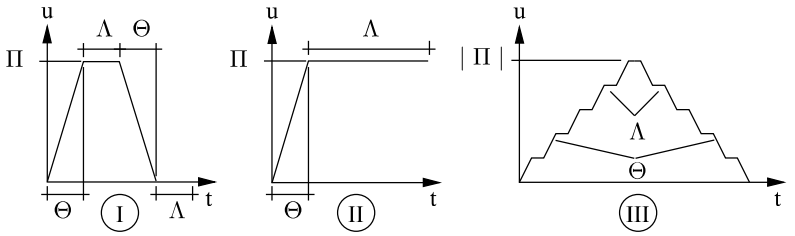

Test	Θ	Λ	Π
Test A	20s	5s	1mm
Test B	2000s	5s	1mm
Test C	2s	86400s	1mm
Test D	2s	10000s	1mm
Test E	2s	10000s	−1mm

Figure 2: Tension compression tests: I–Test A,B; II–Test C; III–Test D,E and u denotes the x component of $\mathbf{u}$

Here we need to mention the sample that was used in all tests. It has an aperture of 12mm and a length of 25mm, where the measurement system is placed. The essential requirement of homogeneous conditions of the sample (see, for example Haupt (2000)) in order to integrate (1) and (2), is given in all tests.

2 Results of the experimental investigation

The data from each test is shown in Figure-3. The first observation we make is the difference of the strength between the batch named KL and both batches dubbed SFB and TS. Secondly, the hardening of the KL batch is nearly linear, ref. tests A and B in Figure-3.

We also see in test A that the relaxation in the 5s hold time starts immediately, an effect that cannot be distinguished in test B because against the long time of loading the 5s hold time shrinks to approximately zero.

The loading part of relaxation test C is driven out very fast, consequently we get a maximum of viscous reaction. After the loading time we hold the elongation of the sample constant to get the relaxation curve. These curves are shown in Figure-3, test C. The information gained from tests C is needed to conduct the step tests (D, E), for which we needed a proper estimation of adequate hold times to be sure that the process of relaxation comes near enough to the equilibrium state. In other words, the forces in the sample seem nearly constant (viz time independent) to the end of hold time. Whether a constant level of force may be assumed or not can be better viewed in the half logarithmic presentation (Figure-3, arrow).

The tests D and E are also shown in Figure-3. These two tests were a challenge for the testing equipment, because the steps of $\Delta u_{\mathrm{step}} = 0.2$mm in 2s tended to dislocate the measurment system, see Al-Baldawi (2009). We think a hold time of t=10000s (Figure-3) is a good compromise to get near enough to the equilibrium state. This is the

general way to come to an equilibrium hysteresis, see Lion et al. (1993) and Lion and Haupt (1994).

Test E works in the compression region. Here, because of the great strength of the KL-batch, many specimens buckled before reaching maximum compression. So, it was impossible to get good measurement results for the KL-batch, which is why it is missing in Figure-3, Test E.

Of course, the palette of experimental investigation tests in material theory and material modelling is much bigger than the five types used here, and all experiments would have better been torsion tests (see. Lion (1994)), but the geometry used depended on the measurment equipment available and the number of specimens was limited.

3 Viscoelastic-plastic Modelling

In literature there are lots of material models that can be used to describe different materials and their behavior under mechanical loading. One of them is a model of Lion (Lion (1994)), which we adjust to our needs and means. The most advantageous feature of Lion's model is its very clear structure concerning the model parameters and experimentally observable phenomena. So, differences in values of identified parameters correlate with differences in the material behavior and thus give a good indicator as to whether the occurrence of a certain material behavior can be depended on or not.

The complete material model is presented in Table-1. The basic idea of it is to split the stress tensor $\mathbf{T}$ into an overstress tensor $\mathbf{T}_{\mathrm{ov}}$, which may as well be a sum of overstress tensors, and an equilibrium state stress tensor $\mathbf{T}_{\mathrm{eq}}$. This ansatz is justified by experimental observations.

The norm used in the equations in the Table-1 is defined for a tensor $\mathbf{A}$ to be: $\|\mathbf{A}\| = \sqrt{\mathbf{A} \cdot \mathbf{A}}$. The notations $\mathbf{A}^K$ and $\mathbf{A}^D$ indicate the splitting of tensor $\mathbf{A}$ into its spherical part $\mathbf{A}^K = \mathrm{tr}(\mathbf{A})\mathbf{1}/3$ and its remaining deviator $\mathbf{A}^D = \mathbf{A} - \mathbf{A}^K$, see Betten (1977).

The overstress tensor $\mathbf{T}_{\mathrm{ov}}$ follows the evolution equation $\dot{\mathbf{T}}_{\mathrm{ov}\,k}$ (Table-1, Overstress), wherein the part $\mathbf{T}_{\mathrm{ov}\,1}$ describes the fast fading overstress and $\mathbf{T}_{\mathrm{ov}\,2}$ stands for slowly fading phenomena. This can be done if the condition for ζ_k is observed and by setting adequate values for the parameters $z_{\mathrm{ov}\,k}$.

The production part of the overstress $\mathbf{T}_{\mathrm{ov}}$ in Lion's model depends on the evolution of the complete strain rate tensor $\dot{\mathbf{E}}$. I.e. the model produces overstress during the whole loading process. This feature was presumably designed by Lion (Lion (1994)) because the material he had to deal with (XCrNi18.9) had extremely viscous properties. This feature proved to be a disadvantage in our material, as we will indicate later on.

To introduce the necessity of the scaling function M it is important to note that the relation between the steady state value of the overstress and the strain rate is given in a nonlinear way, as shown experimentally in Lion (1994). There the steady state overstress values related to several strain rates are given by an exponential ansatz. More general approaches implying a higher effort do not yield to substantial improvements.

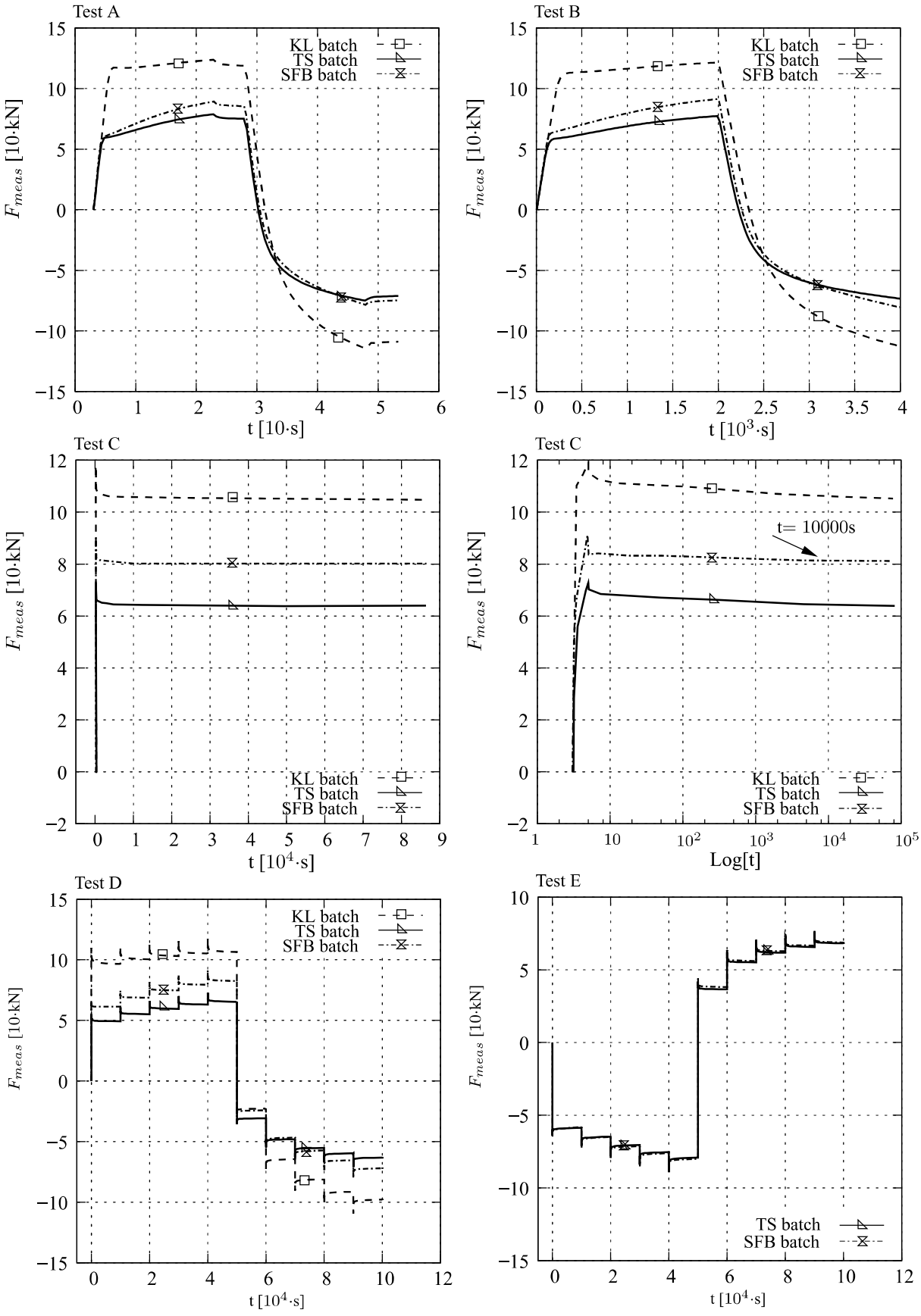

Figure 3: Results – Note that test C is shown in the normal and half logarithm description

Table 1: Complete model of Lion (1994)

Stress splitting	
	$\mathbf{T} = \mathbf{T}_{\mathrm{eq}} + \mathbf{T}_{\mathrm{ov}}$
Overstress	
	$\mathbf{T}_{\mathrm{ov}} = \mathbf{T}_{\mathrm{ov}1} + \mathbf{T}_{\mathrm{ov}2}$
	$\dot{\mathbf{T}}_{\mathrm{ov}k} = \zeta_k \left(2G_{\mathrm{ov}}\dot{\mathbf{E}}^D + 3K_{\mathrm{ov}}\frac{1}{3}\mathrm{tr}(\dot{\mathbf{E}})\mathbf{1} - \dot{\mathbf{T}}_{\mathrm{eq}}\right) - \frac{1}{z_{\mathrm{ov}k}M(\|\mathbf{T}^D_{\mathrm{ov}}\|)}\mathbf{T}_{\mathrm{ov}k}$
Scaling function	
	$M(\|\mathbf{T}^D_{\mathrm{ov}}\|) = e^{\left(-\|\mathbf{T}^D_{\mathrm{ov}}\|/s_0\right)}$
condition for ζ_k	
	$\sum_{k=1}^{2}\zeta_k = 1 \qquad k = 1,2$
Equilibrium state	
	$\mathbf{T}_{\mathrm{eq}} = 2G_{\mathrm{eq}}\left(\mathbf{E}^D - \mathbf{E}_{\mathrm{p}}\right) + 3K_{\mathrm{eq}}\frac{1}{3}\mathrm{tr}(\mathbf{E})\mathbf{1}$
Plastic strain	
	$\dot{\mathbf{E}}_{\mathrm{p}} = \lambda\left(\mathbf{T}^D_{\mathrm{eq}} - \mathbf{X}\right) \qquad \dot{\mathbf{E}}_{\mathrm{pnr}} = \dot{\mathbf{E}}_{\mathrm{p}} - \left(\dot{\mathbf{E}}_{\mathrm{p}} \cdot \frac{\mathbf{X}}{\|\mathbf{X}\|}\right)\frac{\mathbf{X}}{\|\mathbf{X}\|}$
Plastic arc length	
	$\dot{s} = \sqrt{\frac{2}{3}}\|\dot{\mathbf{E}}_{\mathrm{p}}\| \qquad \dot{s}_{\mathrm{nr}} = \sqrt{\frac{2}{3}}\|\dot{\mathbf{E}}_{\mathrm{pnr}}\| \qquad$ Elastic radius σ_0
Hardening	
	$\mathbf{X} = \overline{\mathbf{X}}_k + \widehat{\mathbf{X}} = \overline{\mathbf{X}}_1 + \overline{\mathbf{X}}_2 + \widehat{\mathbf{X}}_1$
Radial	
	$\dot{\overline{\mathbf{X}}}_k = \overline{c}_k\dot{\mathbf{E}}_{\mathrm{p}} - \overline{b}_k\frac{\dot{s}}{1+\overline{\alpha}_{\mathrm{p}}\overline{p}}\overline{\mathbf{X}}_k$
	$\dot{\overline{p}} = \frac{\dot{s}}{\overline{s}_{0\mathrm{p}}\left(1+\alpha_\delta\delta\right)}\left(\|\overline{\mathbf{X}}\| - \overline{p}\right) \qquad \dot{\delta} = \frac{\dot{s}}{\overline{s}_{0\delta}}\left(\overline{p} - \delta\right)$
Nonradial	
	$\dot{\widehat{\mathbf{X}}}_k = \widehat{c}_k\dot{\mathbf{E}}_{\mathrm{pnr}} - \widehat{b}_k\frac{\dot{\widehat{s}}_{\mathrm{nr}}}{1+\widehat{\alpha}\widehat{p}}\widehat{\mathbf{X}}_k$
	$\dot{\widehat{p}} = \frac{\dot{s}_{\mathrm{nr}}}{\widehat{s}_{0\mathrm{p}}}\left(\|\widehat{\mathbf{X}}\| - \widehat{p}\right)$

The experimental investigation was done with elongation controlled tests. So, the strain tensor $\mathbf{E} = \frac{1}{2}\left(\mathrm{grad}\,\mathbf{u} + (\mathrm{grad}\,\mathbf{u})^T\right)$ can be calculated because of the aforementioned conditions of homogeneous deformations of the sample. After decomposing the strain tensor $\mathbf{E}$ in the usual way into an elastic part $\mathbf{E}_{\mathrm{e}}$ and a plastic part $\mathbf{E}_{\mathrm{p}}$, accompanied by an evolution equation $\dot{\mathbf{E}}_{\mathrm{p}}$, Lion describes the equilibrium stress $\mathbf{T}_{\mathrm{eq}}$ with a classic ansatz, see Table-1.

For the reason of experimentally observed higher values of hardening in nonradial processes, Lion included in his model a part called $\mathbf{E}_{\mathrm{pnr}}$, which is perpendicular to the hardening tensor $\mathbf{X}$ and so enlarges the plastic strain $\mathbf{E}_{\mathrm{p}}$. With radial processes, like ours, this feature is not activated and the nonradial hardening tensor $\widehat{\mathbf{X}}$ vanishes as well. This means, in our case, the hardening tensor $\mathbf{X}$ consists only of the radial hardening tensor $\overline{\mathbf{X}}$, see Frederick and Armstrong (2007).

The further functions $\dot{\widehat{p}}$, $\dot{\overline{p}}$ and $\dot{\delta}$ are evolution equations to describe the development of the internal variables $\widehat{p}$, $\overline{p}$ and δ, which can describe the asymmetry between hardening and softening phenomena in steel. Lion et al. (Lion (1994)) found out that the static hysteresis in cyclic tests of stepwise constant amplitude is reached faster, if the steps are increased (hardening tests), than in softening tests (decreasing steps).

To keep a better track, we need to mention the parameter set (3) of the model in Table-1, which has to be identified:

$$\mathbf{p} = (\underbrace{[\zeta_1, \zeta_2, G_{\mathrm{ov}}, K_{\mathrm{ov}}, z_{\mathrm{ov}1}, z_{\mathrm{ov}2}, s_0]}_{\mathbf{T}_{\mathrm{ov}}}, \underbrace{[G_{\mathrm{eq}}, K_{\mathrm{eq}}, \sigma_0]}_{\mathbf{T}_{\mathrm{eq}}}, \underbrace{[\overline{c}_1, \overline{c}_2, \overline{b}_1, \overline{b}_2, \overline{\alpha}_{\mathrm{p}}, \overline{s}_{0\mathrm{p}}, \overline{\alpha}_\delta, \overline{s}_{0\delta}]}_{\overline{\mathbf{X}}}, \underbrace{[\widehat{c}_1, \widehat{b}_1, \widehat{\alpha}, \widehat{s}_{0\mathrm{p}}]}_{\widehat{\mathbf{X}}}) \qquad (3)$$

Finally, we must mention that all the tests carried out in this project (Figure-2) are radial, and that, because of lack of time no cyclic tests could be done, to differentiate between hardening and softening behavior. This means that in the processes available not all the parameters in (3) are activated. For this reason we have to reduce the material model (Table-1) in a physically correct way.

3.1 9-Parameter Model

In radial tests there is no need for $\mathbf{E}_{\mathrm{pnr}}$, and there is even no possibility to identify the parameters belonging to the nonradial hardening equations, because there is no experimental data. For this reason the hardening tensor can be described only by its radial part

$$\mathbf{X} = \overline{\mathbf{X}}. \tag{4}$$

As mentioned above, there were no cyclic tests, so there is no data form wich we can glean the hysteresis behavior of 51CrV4. Therefore we set the evolution equation for the internal variable $\overline{p}$ to zero. With this follows

$$\overline{\alpha}_{\mathrm{p}}\overline{p} = \alpha_p \qquad \text{and} \qquad b_\alpha = \frac{b}{1+\alpha_{\mathrm{p}}} \tag{5}$$

and the hardening equation becomes the well-known Armstrong-Frederick-ansatz.

We limit the overstress evolution equation to one summand, and having to hold the condition for ζ (Table-1) means the evolution equation for $\mathbf{T}_{\mathrm{ov}}$ is described by

$$\dot{\mathbf{T}}_{\mathrm{ov}} = 2G_{\mathrm{ov}}\dot{\mathbf{E}}^D + 3K_{\mathrm{ov}}\frac{1}{3}\mathrm{tr}(\dot{\mathbf{E}})\mathbf{1} - \dot{\mathbf{T}}_{\mathrm{eq}} - \frac{1}{z_{\mathrm{ov}}M(\|\mathbf{T}^D_{\mathrm{ov}}\|)}\mathbf{T}_{\mathrm{ov}}. \tag{6}$$

Finally, we line up all equations, as previously done, in Table-2, accompanying it with the appropriate parameter set $\mathbf{p}_{9p}$:

$$\mathbf{p}_{9\mathrm{p}} = (\underbrace{[G_{\mathrm{ov}}, K_{\mathrm{ov}}, z_{\mathrm{ov}}, s_0]}_{\mathbf{T}_{\mathrm{ov}}}, \underbrace{[G_{\mathrm{eq}}, K_{\mathrm{eq}}, \sigma_0]}_{\mathbf{T}_{\mathrm{eq}}}, \underbrace{[c, b_\alpha]}_{\mathbf{X}}). \tag{7}$$

Table 2: 9-Parameter Model

Stress splitting	
	$\mathbf{T} = \mathbf{T}_{\mathrm{eq}} + \mathbf{T}_{\mathrm{ov}}$
Overstress	
	$\mathbf{T}_{\mathrm{ov}} = \mathbf{T} - \mathbf{T}_{\mathrm{eq}}$
	$\dot{\mathbf{T}}_{\mathrm{ov}} = 2G_{\mathrm{ov}}\dot{\mathbf{E}}^D + 3K_{\mathrm{ov}}\frac{1}{3}\mathrm{tr}(\dot{\mathbf{E}})\mathbf{1} - \dot{\mathbf{T}}_{\mathrm{eq}} - \frac{1}{z_{\mathrm{ov}}M(\|\mathbf{T}^D_{\mathrm{ov}}\|)}\mathbf{T}_{\mathrm{ov}}$
Scaling function	
	$M(\|\mathbf{T}^D_{\mathrm{ov}}\|) = e^{\left(-\|\mathbf{T}^D_{\mathrm{ov}}\|/s_0\right)}$
Equilibrium State	
	$\mathbf{T}_{\mathrm{eq}} = 2G_{\mathrm{eq}}\left(\mathbf{E}^D - \mathbf{E}_{\mathrm{p}}\right) + 3K_{\mathrm{eq}}\frac{1}{3}\mathrm{tr}(\mathbf{E})\mathbf{1}$
Plastic strain	
	$\dot{\mathbf{E}}_{\mathrm{p}} = \lambda\left(\mathbf{T}^D_{\mathrm{eq}} - \mathbf{X}\right)$
Plastic arc length	
	$\dot{s} = \sqrt{\frac{2}{3}}\|\dot{\mathbf{E}}_{\mathrm{p}}\|$ Elastic radius σ_0
Hardening	
	$\mathbf{X} = \overline{\mathbf{X}}$
Radial	
	$\dot{\mathbf{X}} = c\dot{\mathbf{E}}_{\mathrm{p}} - b_\alpha\dot{s}\mathbf{X}$

Two problems are still unsolved. The first one is to determine the proportionality factor λ of the normality rule

$$\mathbf{f}_\sigma = \frac{\partial F}{\partial \mathbf{T}_{\mathrm{eq}}} = \mathbf{T}^D_{\mathrm{eq}} - \mathbf{X}, \tag{8}$$

see Table-1. The second problem is the transverse strain in the sample because elongation controlled processes are not completely strain controlled. However, the process has to fulfill a combination of boundary conditions in stress and strain. So, the transverse strain is governed by the material behavior.

The proportionality factor The yield function of v. Mises is given by

$$F = \mathrm{II}_{\mathbf{f}_\sigma} - \frac{2}{3}\sigma_0^2 = 0, \tag{9}$$

where $\mathrm{II}_{\mathbf{f}_\sigma}$ is the second invariant of $\mathbf{f}_\sigma$ and can be calculated as follows:

$$\mathrm{II}_{\mathbf{f}_\sigma} = \mathbf{f}_\sigma \cdot \mathbf{f}_\sigma.$$

The yield function (9) is an essential instrument of the plasticity theory, another example is shown in Kreissig and Grewolls (1995). It can be interpreted as a surface which divides the stress space into an elastic $(F < 0)$ and plastic region $(F = 0)$, see Haupt (1977). The restraint for $\mathbf{T}_{\mathrm{eq}}$ to never leave the yield surface in outward direction leads to the consistency condition $\dot{F} = 0$, see Haupt (2000),

$$\dot{F} = \mathbf{f}_\sigma \cdot \left(\dot{\mathbf{T}}_{\mathrm{eq}} - \dot{\mathbf{X}}\right) = 0. \tag{10}$$

With a hardening ansatz as in Table-2, the plastic arc length s, and the plastic strain rate $\dot{\mathbf{E}}_{\mathrm{p}}$, respectively, the consistency condition (10) becomes the equation to determine λ with:

$$\lambda = \frac{1}{\alpha}\frac{\dot{B}}{\mathbf{f}_\sigma \cdot \mathbf{f}_\sigma}. \tag{11}$$

For the concise form of (11) we use the abbreviations:

$$\alpha = c - b_\alpha \mathbf{f}_\sigma \cdot \mathbf{X}\sqrt{\frac{2}{3}\frac{1}{\mathbf{f}_\sigma \cdot \mathbf{f}_\sigma}}, \tag{12}$$

$$\text{and} \quad \dot{B} = \mathbf{f}_\sigma \cdot \dot{\mathbf{T}}_{\mathrm{eq}} > 0. \tag{13}$$

Equation (13) is called loading condition, see Haupt (2000).

Transverse strain The transverse strain can be calculated from the fact that the stress tensor as well as its rate are non zero only in component $\mathbf{T}_{11} = \sigma_{xx}$, or $\dot{\mathbf{T}}_{11} = \dot{\sigma}_{xx}$, respectively. On the other hand, due to isotropy, the strain tensor $\mathbf{E}$ only has the components $\mathbf{E}_{11} = e_a$ and $\mathbf{E}_{22} = \mathbf{E}_{33} = e_b$. This leads to two differential equations for e_b and the corresponding component of the overstresses $\mathbf{T}_{\mathrm{ov}\,22} = \mathbf{T}_{\mathrm{ov}\,33} = s_b$.

The thus completed 9-parameter model is mainly used for first numerical studies and to get some first indications of the way single parameters would evolve. But, as can be seen in the Figures 5–9, the simple Armstrong-Frederic-ansatz used here is not sufficient to describe the observed material behavior (compare the hourglas and triangle lines).

3.2 11-Parameter Model

After the disappointing results of the hardening behavior of the 9-parameter model we found a solution by doubling the number of production terms in the sum of the radial hardening, while setting the limiting term of the second summand to zero, see Lion and Haupt (1994):

$$\mathbf{X}_{\mathrm{new}} = \mathbf{X}_{\mathrm{simple}} + \mathbf{X}_{\mathrm{add}}. \tag{14}$$

In the equation above, $\mathbf{X}_{\mathrm{simple}}$ is the usual Armstrong-Frederick-Ansatz, see Table-2, enhanced by another Armstrong-Frederick-type tensor $\mathbf{X}_{\mathrm{add}}$, which will increase linearly, if parameter $b_{\alpha\,\mathrm{add}}$ is set to zero, see Figure-4. This ansatz yields a smooth run into the simulated curves, see Figures 5–9. The same effect can also be viewed in figure-4 for the components of hardening tensor.

Again, in Table-3, we line up all equations for the new hardening ansatz, as well as the extended parameter set $\mathbf{p}_{11p}$:

$$\mathbf{p}_{11\mathrm{p}} = (\underbrace{[G_{\mathrm{ov}}, K_{\mathrm{ov}}, z_{\mathrm{ov}}, s_0]}_{\mathbf{T}_{\mathrm{ov}}}, \underbrace{[G_{\mathrm{eq}}, K_{\mathrm{eq}}, \sigma_0]}_{\mathbf{T}_{\mathrm{eq}}}, \underbrace{[c_{\mathrm{simple}}, b_{\alpha\,\mathrm{simple}}, c_{\mathrm{add}}, b_{\alpha\,\mathrm{add}}]}_{\mathbf{X}}), \tag{15}$$

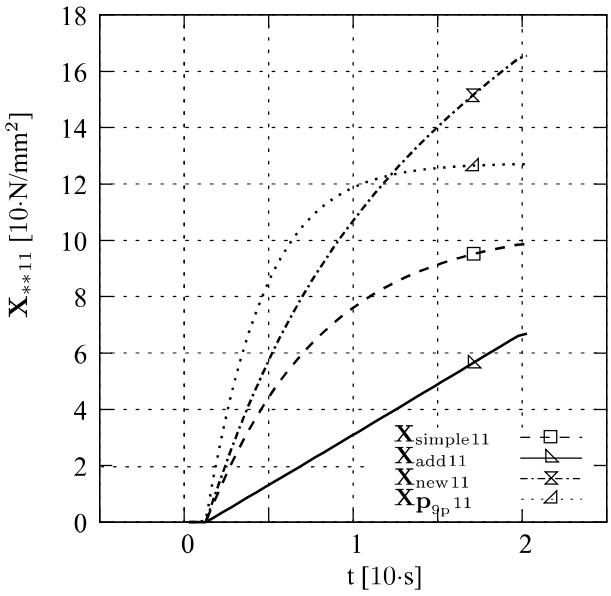

Figure 4: Satiation of the hardening ansatz for the TS batch – Test A

and Table-4. For this we used the facts:

$$2G = \frac{E}{1+\nu} \qquad \text{and} \qquad 3K = \frac{E}{1-2\nu}. \tag{16}$$

Table 3: 11-Parameter Model

Hardening	
	$\mathbf{X} = \mathbf{X}_{\text{new}} = \mathbf{X}_{\text{simple}} + \mathbf{X}_{\text{add}}$
Radial:	
	$\dot{\mathbf{X}}_{\text{simple}} = c_{\text{simple}}\dot{\mathbf{E}}_{\text{p}} - b_{\alpha\text{simple}}\dot{s}\mathbf{X}_{\text{simple}}$
	$\dot{\mathbf{X}}_{\text{add}} = c_{\text{add}}\dot{\mathbf{E}}_{\text{p}} - b_{\alpha\text{add}}\dot{s}\mathbf{X}_{\text{add}}$ with $b_{\alpha\text{add}} \approx 0$

Table 4: Values of the parameters

Charge:			SFB	TS	KL
Overstress					
Elastic part	E_{ov}	[N/mm^2]	227000	226900	221050
	ν_{ov}	[1]	0.372	0.366	0.355
Scaling function	s_0	[N/mm^2]	9.9	7.0	16.5
	z_0	[s]	348	374	425
Equilibrium state					
Elastic radius	σ_0	[N/mm^2]	490	462	835
Elastic part	E_{eq}	[N/mm^2]	208800	204200	201100
	ν_{eq}	[1]	0.370	0.365	0.353
Hardening					
	c_{simple}	[N/mm^2]	11060	8033	17674
	$b_{\alpha\text{simple}}$	[1]	75.2	76.4	111.9
	c_{add}	[N/mm^2]	2649	1837	861
	$b_{\alpha\text{add}}$	[1]	$\rightarrow$0	$\rightarrow$0	$\rightarrow$0

4 Comparison with the experimental investigation

Because of the extended hardening model, the 11-parameter model gives a better representation of the real material behavior our results got using 9 parameters. But, as can be seen in Figure-6, the best results are coupled with the slowest processes which indicates that the overstress production of the model is too sensitive near the elastic-plastic transit, a phenomenon that increases with faster loading. The results for slow loading are better because the process stays near the equilibrium state, which is modelled classically.

The simulations for all the other tests are unsatisfying, because here the overstress ansatz exaggerates. This shortcoming cannot be put right. Even by expanding the ansatz with a second summand, there was no improvement:

$$\mathbf{T}_{\mathrm{ov}} = \mathbf{T}_{\mathrm{ov1}} + \mathbf{T}_{\mathrm{ov2}}. \tag{17}$$

The cause of this symptom is the overstress production depending on the whole strain, which would be adequate if the material investigated would show distinctive viscoelastic behavior. But this cannot be observed. It would have been better to have used a viscoplastic model, see Haupt (1996), Olschewski (1996), Chaboche (1989) and Chaboche (2008).

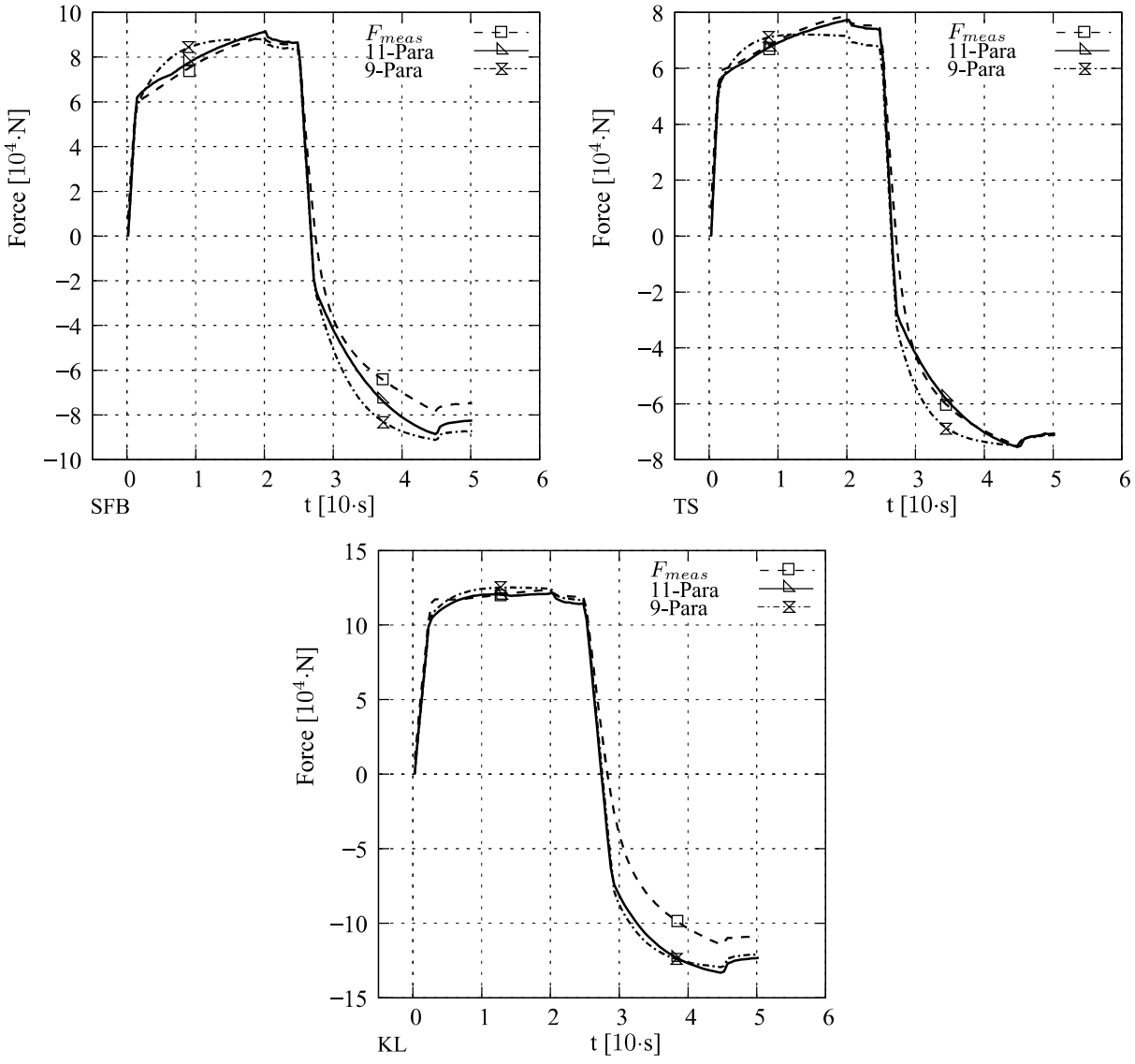

Figure 5: Test A (fast loading)

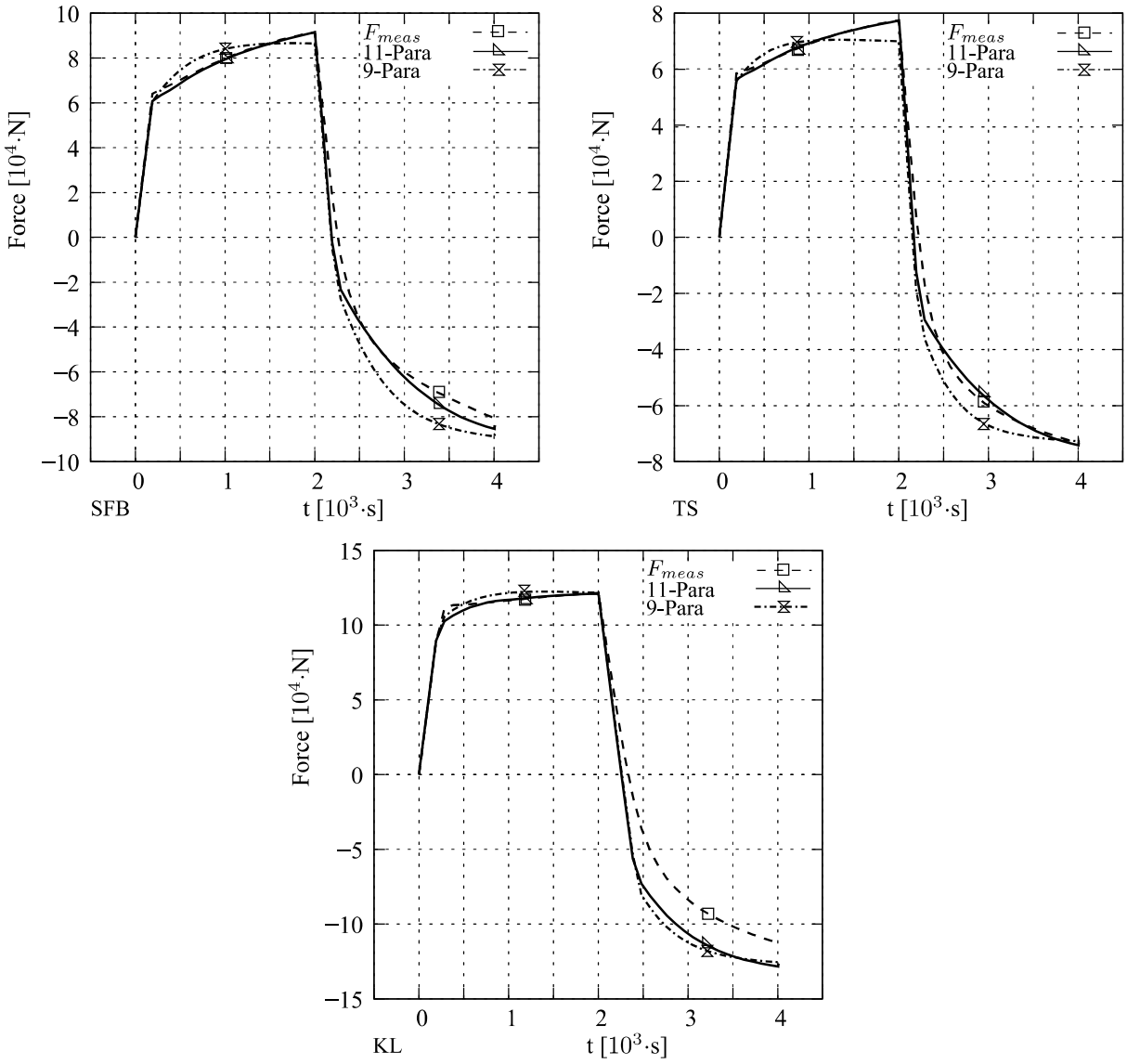

Figure 6: Test B (slow loading)

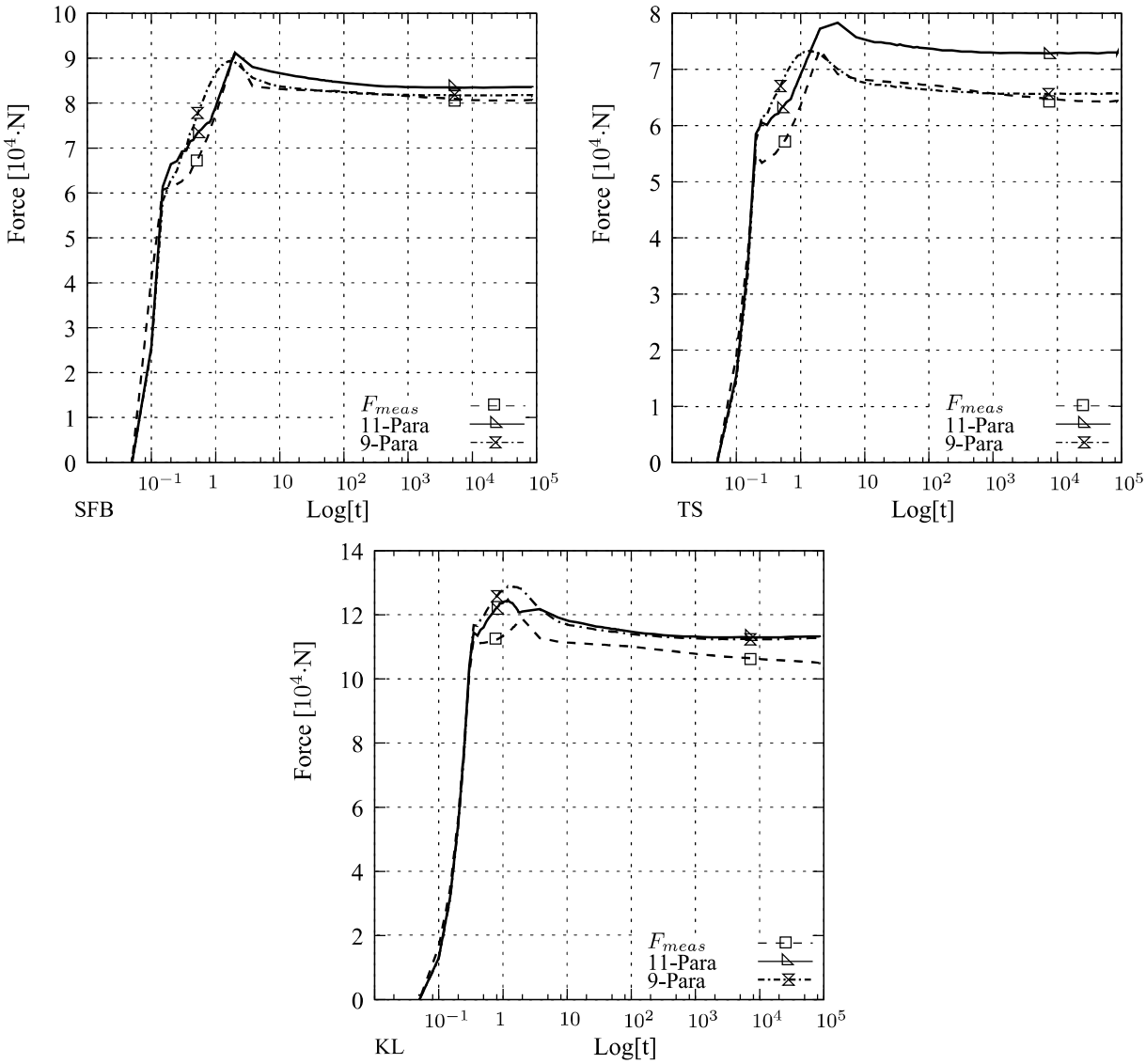

Figure 7: Test C (relaxation, fast loading)

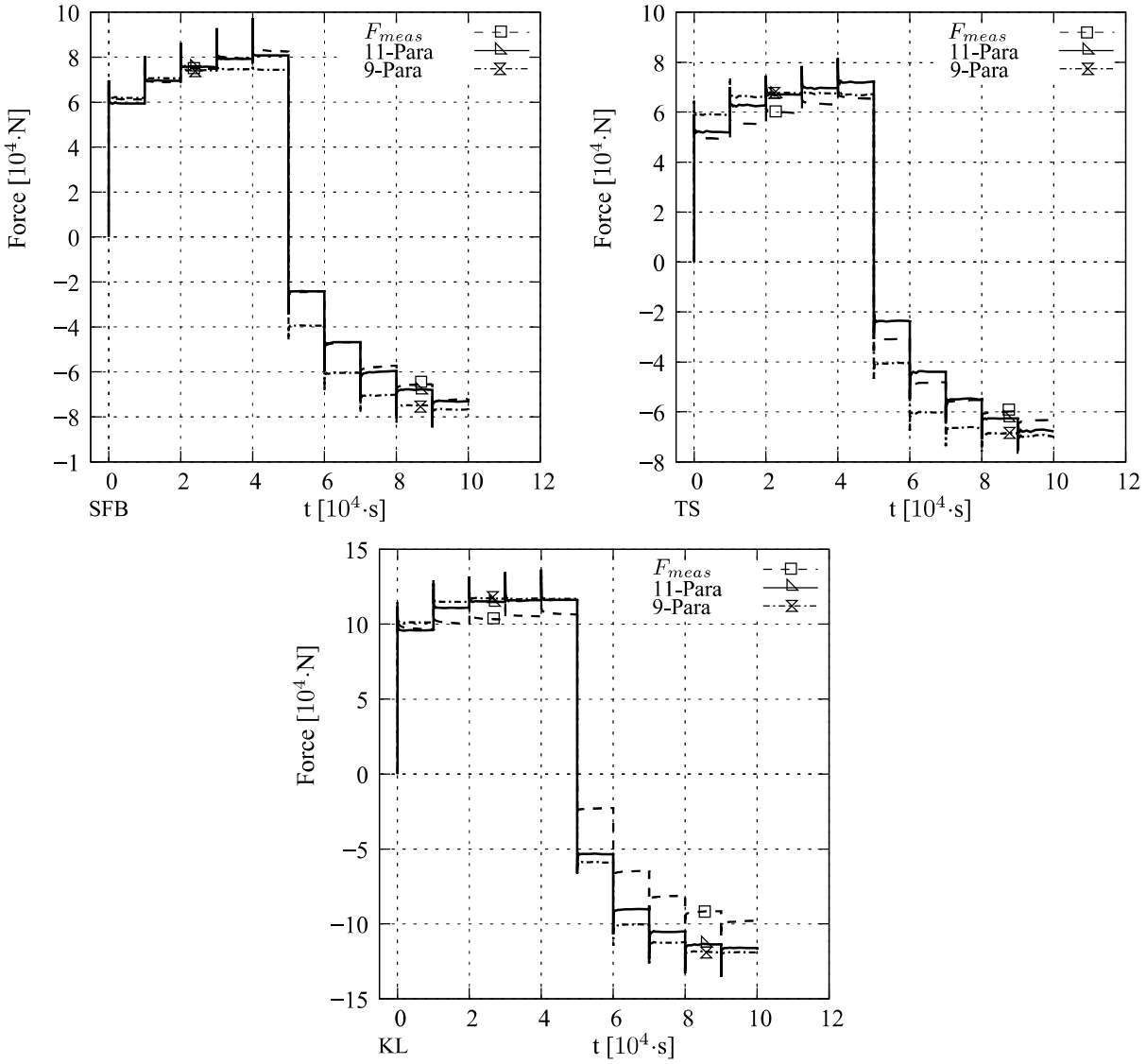

Figure 8: Test D (stepwise fast loading/relaxation – tension)

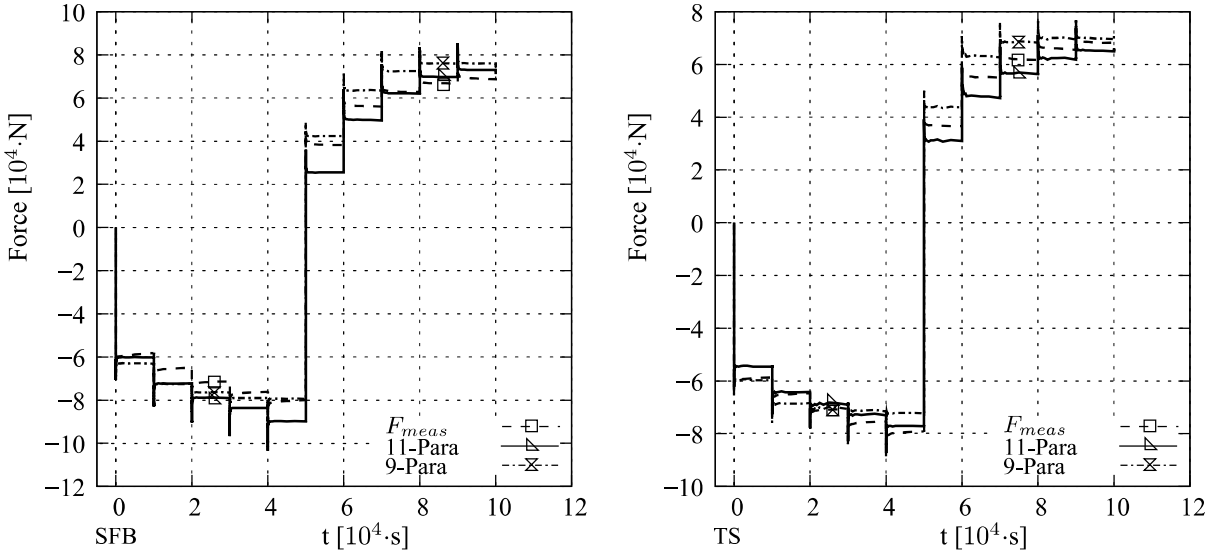

Figure 9: Test E (stepwise fast loading/relaxation – compression)

5 Conclusions

The experimental investigation showed three different answers for the three batches under the same mechanical loading – in the case of the KL batch distinctly different, especially in the elastic region and in the hardening behavior. Such seemingly random discrepancies pose a great disadvantage for engineering needs, because e.g. for a metal forming engineer it would be a challenge to shape KL batch material instead of the SFB or TS type, whereas for a design engineer a salient elastic part is required, as can be found in KL.

Table-5 shows the differences between the parameter sets and makes clear how big the discrepances in the individual parameters can be.

The average value is calculated by

$$\Phi^{\mathrm{avg}} = \frac{1}{n}\sum_{i}^{n}\Phi_i \quad ; \quad n = 3 \quad (\mathrm{SFB}, \mathrm{TS}, \mathrm{KL}) \tag{18}$$

and the relative error by

$$\Delta\Phi = \left(\frac{\Phi_i - \Phi^{\mathrm{avg}}}{\Phi^{\mathrm{avg}}}\right) \cdot 100\%. \tag{19}$$

Table 5: Comparison of the parameter sets

Batch			Avereage	△ SFB [%]	△ TS [%]	△ KL [%]
Overstress						
Elastic part	E_{ov}	[N/mm^2]	224984	1	1	-2
	ν_{ov}	[1]	0.364	2	1	-3
Scaling function	s_0	[N/mm^2]	11.14	-11	**-37**	**48**
	z_0	[s]	382.2	-9	-2	11
Equilibrium state						
Elastic radius	σ_0	[N/mm^2]	595.67	**-18**	**-22**	**40**
Elastic part	E_{eq}	[N/mm^2]	204702	2	0	-2
	ν_{eq}	[1]	0.362	2	1	-3
Hardening						
	c_{simple}	[N/mm^2]	12255.5	-10	**-35**	**44**
	$b_{\alpha\mathrm{simple}}$	[1]	87.82	-14	-13	**27**
	c_{add}	[N/mm^2]	1782.27	**49**	3	**-52**
	$c_{\mathrm{simple}} + c_{\mathrm{add}}$	[N/mm^2]	14037.8	-2	**-30**	**32**

The one and only material property found to be the same in all batches is elasticity, represented by the parameters E_{ov}, E_{eq}, ν_{ov}, and ν_{eq}. The borderline between elastic and plastic behavior (elastic radius σ_0) however, shows the first big difference, in this setting the KL-batch aside from both the others. The same applies to the limiting term $b_{\alpha\mathrm{simple}}$, best seen in Table-4.

The evolution of hardening at the first onset of plastic deformation is governed by both, c_{simple} and c_{add}. A comparison of these parameters (last line Table-5) is not quite as decisive as the ones above because here all batches differ in the same way as parameter s_0 of the scaling function does: the plastic hardening properties of all batches seem to be different. The viscous properties again, as seen in relaxation, are quite comparable in all three batches, see parameter z_0.

If material behavior differs, in such wide range, under mechanical loading is modelled using one and the same model, the ensuing identification will lead to the different parameter sets, if all batches are treated separately, as done here. On the other hand, to identify one set of parameters using the experimental data of all batches simultaniously would be the same nonsense as to average the parameters found for all batches in order to reach a one-for-all parameter set, see Table-5. There is no way to find a parameter set for a certain model and a material e.g.

called 51CrV4, that could be published and used by others – any batch delivered needs to have its own parameters identified.

Acknowledgements This work was relevantly supported by Prof. Dr.-Ing. O. Wünsch (University of Kassel). We also thank Transregio 30 for furnishing the material dubbed SFB.

References

Al-Baldawi, A.: Identifikation der Materialparameter eines viskoelastisch-plastischen Materialmodells anhand experimenteller Daten aus einaxialen Versuchen. Vergleich von drei verschiedenen Chargen 51CrV4 (2009), Diplomarbeit, Universität Kassel.

Betten, J.: *Elementare Tensorrechnung für Ingenieure*. Vieweg, Wiesbaden (1977).

Chaboche, J. L.: Constitutive equations for cyclic plasticity and cyclic viscoplasticity. *International Journal of Plasticity*, 5-3, (1989), 247–302.

Chaboche, J. L.: A review of some plasticity and viscoplasticity constitutive theories. *International Journal of Plasticity*, 24-10, (2008), 1642–1693.

Chakrabarty, J.: *Theory of Plasticity*. Elsevier, Amsterdam (2006).

Frederick, C.; Armstrong, P.: A mathematical representation of the multiaxial Bauschinger effect . *Materials at High Temperatures*, 24-1, (2007), 1–26.

Haupt, P.: *Viskoelastizität und Plastizität*. Springer, Berlin (1977).

Haupt, P.: Konzepte der Materialtheorie. *Technische Mechanik*, 16-1, (1996), 13–22.

Haupt, P.: *Continuum Mechanics and Theory of Materials*. Springer, Berlin (2000).

Kreissig, R.: Parameteridentifikation inelastischer Deformationsgesetze. *Technische Mechanik*, 16-1, (1996), 97–106.

Kreissig, R.; Grewolls, G.: Distortional hardening within a cubic yield theory. *Technische Mechanik*, 15-4, (1995), 333–339.

Lion, A.: Materialeigenschaften der Viskoplastizität (1994), Dissertation, Universität Kassel.

Lion, A.; Haupt, P.: Experimentelle Identifikation und mathematische Modellierung von Materialeigenschaften der Viskoplastizität. *Z. angew. Math. Mech.*, 74, (1994), 10–13.

Lion, A.; Haupt, P.; Schreiber, L.: Experimentelle Untersuchung des geschwindigkeitsabhängigen Materialverhaltens bei nichtradialen Belastungen. *Z. angew. Math. Mech.*, 73, (1993), 320–325.

Olschewski, J.: Viskoplastische Materialmodellierung und Anwendungen im Gasturbinenbau. *Technische Mechanik*, 16-1, (1996), 39–50.

Schreiber, L.: Parameteridentifikation bei Stoffmodellen mit der Evolutionsstrategie. *Z. angew. Math. Mech.*, 73, (1993), 343–345.

Svendsen, B.: On the Continuum Mechanics of Elastic and Inelastic Simple Materials. *Technische Mechanik*, 16-1, (1996), 1–12.

Address: Dipl.-Ing. Ammar Abid (Al-Baldawi), Institute of Mechanics, University of Kassel, D-34125 Kassel
email: ammar@uni-kassel.de